Quantum Chemistry Study of Fullerene and Carbon Nanotube Fluorination

Richard L. Jaffe

NASA Ames Research Center, Moffett Field, California 94035

Received: December 19, 2002; In Final Form: June 26, 2003

The reaction of fullerenes and carbon nanotubes with molecular fluorine has been studied using B3LYP calculations. The nanotube substrates are represented by model polycyclic aromatic hydrocarbons that are constrained to have nonplanar geometries with curvatures corresponding to (10,10), (5,5), and (16,0) nanotubes. Most of the calculations for fullerenes are carried out for C_{60}. The calculations are focused on the addition of one to four F-atoms to the fullerene or nanotube substrate. The preferred binding sites for sequential fluorine addition are studied along with the geometry deformations experienced by the substrate. For C_{60}, a strong preference exists for pairwise addition to the C−C double bonds between pentagons (denoted 6/6 addition). Subsequent addition to neighboring 6/6 bonds is also favored. These results are in agreement with recent experimental data. For addition of F_2 to armchair nanotubes, the favored product has the fluorine atoms bonded to adjacent carbons with an orientation perpendicular to the tube axis, whereas for zigzag nanotubes the favored orientation is parallel to the tube axis. However, in the latter case a second product with the fluorine atoms at the 1−4 positions of a hexagon, but still parallel to the tube axis, is less than 0.8 kcal/mol higher in energy. The binding energy of a pair of fluorine atoms to C_{60} is 115 kcal/mol, which is greater than the value found for any of the nanotube model molecules. Zigzag nanotubes are found to form more stable fluorination products than armchair tubes of comparable diameter (83 kcal/mol for (16,0) compared to 76 kcal/mol for (10,10) for addition of F_2). However, smaller diameter nanotubes such as the (5,5) armchair tube have even higher binding energies (91 kcal/mol for addition of F_2). For C_{60} and (10,10) nanotubes, addition of a second F-atom pair results in higher binding energies per F-atom than is found for the first pair. Limited calculations have been carried out to estimate the energy barriers for the fluorination process.

1. Introduction

Since the first characterization of fullerenes in 1985[1] and both multiwall (MWNT) and single-wall carbon nanotubes (SWNT) in the early 1990s,[2,3] chemists have been fascinated by the structure and properties of this so-called third form of carbon. Commercial applications, however, have been slow to develop. Fullerenes have been considered for use as lubricants,[4] superconductors,[5] and drug delivery agents.[6] Nanotubes have electronic and mechanical properties that make them potential candidates for nanoelectronic devices[7] (including molecular electronics) and nanocomposite materials.[8] Development of a controlled functionalization chemistry for nanotubes would facilitate their use in some of these applications.

Fullerenes and carbon nanotubes (CNT) are known to be quite stable chemically because they are composed entirely of a network of sp^2-hybridized carbon atoms.[9] Chemical modification requires either the breaking of that network (e.g., fulleroid formation) or the conversion of some of the carbon atoms to sp^3 hybridization. Either possibility carries with it a significant energy cost and requires a large distortion of the original fullerene and nanotube geometry. Nonetheless, fullerene molecules (e.g., C_{60} and C_{70}) have been shown to undergo a variety of chemical reactions such as cycloadditions[10] and radical additions.[11] Some of the most widely studied reactions involving C_{60} and higher fullerenes are fluorination with F_2, rare gas fluorides, and metal fluorides (for excellent reviews see Taylor[12] and Boltalina[13]). Using mass spectrometry, IR and ^{19}F NMR spectroscopy, many products of fullerene fluorination have been characterized. For C_{60}, major fluorination products include $C_{60}F_{48}$, $C_{60}F_{36}$, and $C_{60}F_{18}$, but many minor products from $C_{60}F_2$ to $C_{60}F_{20}$ have also been identified. Taylor[12] has made the following generalizations: (1) fluorine atoms tend to add in pairs to across the double bonds that radiate from the fullerene pentagons, (2) reaction proceeds as long as the aromaticity of the substituted fullerene is increased and (3) further reaction beyond $C_{60}F_{48}$ is inhibited by steric effects. The first publications reporting production of $C_{60}F_{48}$ by reaction with F_2 and KrF_2 are refs 14 and 15, respectively. Use of metal fluoride reagents such as MnF_3 were first reported in 1996 by Boltalina et al.[16] and led to major products $C_{60}F_{36}$ and $C_{60}F_{18}$. More recently, $C_{60}F_2$[17,18] and $C_{60}F_x$ with $x = 4-8$[19] were identified as minor products in the reaction of C_{60} with K_2PtF_6. In general, the sidewalls of carbon nanotubes have proved to be much less reactive. Although nanotube ends and defect sites are known to be readily oxidized, forming hydroxyl and carboxyl groups, the best evidence to date for successful chemical modification of CNT sidewalls is for reaction with F_2 to form stable highly fluorinated products.[20−22] Smalley and co-workers[21] have produced and characterized SWNT samples with over 50% fluorination simply by mixing the nanotube sample with F_2 (gas) at 400 °C for 13 h. This is similar to an older approach used for fluorination of graphite (cf., refs 23 and 24). For lower degrees of fluorination, the reaction is reversible and the degree of fluorination varies linearly with reaction time. The greater degree of fluorination results in irreversible damage to the nanotube sample. In addition, this fluorinated nanotube product reacts reversibly with alkyllithium and magnesium Grignard reagents to substitute alkyl groups for fluorine atoms.[25] The combination of fluorination plus substitution reactions might

10.1021/jp027778m
Published on Web 08/30/2003

serve as an effective route to creating arbitrarily functionalized nanotubes with tailored chemical properties. However, in this process there is no control of the distribution of adducts on the nanotube sidewall. Halas, Scuseria, and their co-workers[26] have studied fluorinated nanotubes using high resolution STM imaging. They report the formation of circumferential bands with apparently complete fluorination along the length of the nanotube. In that work,[26] semiempirical AM1 calculations for patterned reaction products (such as zigzag rows of attached F-atoms) indicated only small energetic preferences for specific patterns.

Semiempirical MO calculations of substituted C_{60} have been carried out by Matsuzawa et al.[27] who considered $C_{60}X_n$ with X = H or halogens and n taking even values between 2 and 60. More recently, Clare and Kepert reported extensive AM1 calculations of $C_{60}H_n$ and $C_{60}F_n$ for $n > 36$[28] and for $C_{70}F_{38}$ and $C_{70}F_{40}$.[29] All of these studies have shown that the structures of hydrogenated and fluorinated fullerenes are similar. The results of more limited calculations have also been published by Fowler and co-workers for $C_{60}Cl_{10}$[30] and $C_{60}Br_8$.[31] This work sheds some light on the preferences between halogen atom substitution at adjacent carbon sites (denoted 1−2 adducts) and more widely spaced products (denoted 1−4 adducts). For small adducts such as H and F atoms, there is no steric hindrance and 1−2 adducts are formed, but for larger adducts such as Cl and Br, 1−4 products are preferred. It is also seen that subsequent hydrogen and fluorine addition favors C−C double bonds adjacent to the prior addition sites.

The first ab initio quantum chemistry study of fullerene radical addition products is by Cahill and Rohlfing[32] for $C_{60}H_x$. Similarly, Jaffe[33] has studied various fullerene and nanotube cycloaddition products using similar methods. Recently, Bauschlicher[34−36] used the ONIOM method[37] to study hydrogenation and fluorination products of a (10,0) nanotube. In that work, sequential addition occurred adjacent to substituted carbons for 2−4 fluorine atoms and the products with even numbers of fluorine or hydrogen atoms were preferred. A computational study by Kudin et al.[38] considered highly fluorinated (10,10) and (18,0) nanotubes with stoichiometry C_2F. They employed periodic local spin density and density functional methods for five different fluorination patterns and found the most stable one to be lines of fluorine atoms parallel to the tube axis for the armchair nanotube and a helical arrangement for zigzag tubes.

Though it is evident that carbon nanotubes are less reactive than fullerene molecules, the underlying reason for this differing reactivity is not clear. In the case of fullerenes, the localized nature of the C−C bonds facilitates addition to the π bond. It is also possible that upon sp^2 to sp^3 conversion, the deformation energy required to make the carbon atom tetrahedral is less than in the nanotube case because the fullerene starts with larger distortions from trigonal carbon. If the latter factor were significant, one would expect the reactivity of nanotubes to vary with their diameter and chirality, because the trigonal carbon structure of smaller diameter tubes is more distorted. Quantum chemistry calculations should be able to test these hypotheses.

To date, the quantum chemistry studies of fullerene functionalization products[32,33] are consistent with experimental findings without exception. For the hydrogenation and cycloaddition cases studied, the calculations confirm the stability of specific products for the corresponding reactions carried out in the laboratory. This is a noteworthy achievement because the calculations have been carried out for isolated (i.e., gas phase) systems whereas the experimental data are all for reactions occurring in solution. However, there have not been definitive experimental results for nanotube functionalization other than fluorination[20−22] that could be compared with computational studies. In the present work, quantum chemistry calculations are carried out to study the fluorination of fullerenes and nanotubes. As products have been prepared in the laboratory in both cases, this work will help set threshold limits for the stability of products of other possible nanotube functionalization reactions.

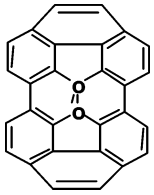

Figure 1. Model molecule ($C_{30}H_{12}$) for small fullerenes. The attachment sites for the E*2F6/6* adduct are marked **o**.

In the next section, our computational protocol for studying fullerene and nanotube functionalization products is presented. Sections 3 and 4 present the results of the quantum chemistry calculations for fullerenes and nanotubes, respectively. Addition of one to six fluorine atoms to the fullerene and nanotube substrates is examined. Section 5 briefly presents results for the fluorination of planar graphene. These results are discussed and compared in section 6 and conclusions are presented in section 7.

2. Methods

Owing to the large size of fullerene molecules and complete segments of nanotubes, it is not always practical to carry out ab initio quantum chemistry calculations on the complete molecules. In this work, we utilize model hydrocarbon molecules to represent pieces of the fullerene or nanotube being studied. In some of the calculations the complete C_{60} molecule is used, whereas in others small curved fullerene fragments are used as models to represent C_{60} and larger fullerenes. For example, the (1−1) pentagon pair[39] surrounded by a ring of eight hexagons, shown in Figure 1, has a curvature similar to that of the equivalent fragment removed from a C_{60} molecule. Various polycyclic aromatic hydrocarbons (PAH) with curvature maintained by external constraints are used as model molecules for armchair (10,10) and zigzag (16,0) single-wall carbon nanotubes. All-hexagon PAH models were used to represent the tube sidewalls and PAH model molecules containing a single pentagon were used to represent the tip of a nanotube endcap. An example of the (10,10) nanotube sidewall model extracted from a section of the actual nanotube is shown in Figure 2. All the fullerene and nanotube model molecules have hydrogen atoms added to the perimeter carbons to terminate dangling bonds.

Product geometries and adduct binding energies are obtained for addition of one to six fluorine atoms. In this work, we use the following notation for the total binding energy:

$$\mathrm{E}n\mathrm{F}type = \mathrm{E}(\mathrm{substrate}\bullet\mathrm{F}_n) - \mathrm{E}(\mathrm{substrate}) - n\mathrm{E}(\mathrm{F})$$

where n is the number of fluorine atoms in the product and *type* is a label describing the arrangement of the fluorine adducts. For example, E*2F1−4trans* denotes the binding energy of a fluorination product with two F-atoms added to 1−4 positions on the substrate at the end carbon atoms of a C_4 chain with a trans or zigzag arrangement. Detailed descriptions of all fluorination products studied are given in sections 3 and 4.

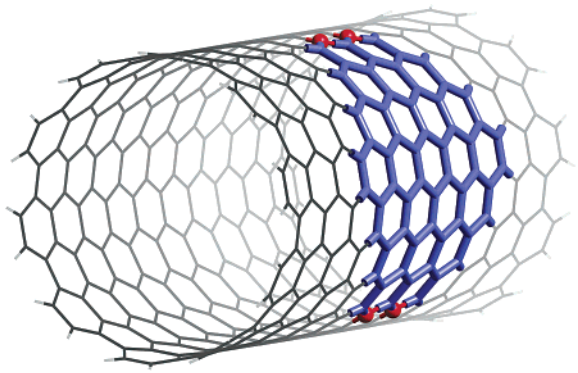

Figure 2. Large model molecule ($C_{64}H_{20}$) for (10,10) carbon nanotube as extracted from a complete carbon nanotube segment. Thick blue atoms and bonds are carbon atoms in the model molecule. The red balls represent carbon atoms that are fixed in the geometry optimization to maintain the nanotube curvature.

The calculations utilized density functional theory (DFT)[40] with a widely used hybrid nonlocal-functional (B3LYP) developed by Becke[41] and parametrized by Stephens et al.[42] Use of this functional has been found to reproduce bond lengths and angles to within 0.03 Å and 0.5−1.0° and bond energies to within ±3 kcal/mol for a wide range of molecules. It also reproduces the experimental structures and energy differences in naphthalene and azulene.[39] The B3LYP/6-31G(d) 298 K enthalpy difference between azulene and naphthalene is 33.6 kcal/mol compared to the experimental difference in standard heats of formation of 37.5.[43] On the basis of extensive tests, it was determined that geometry optimization of the model molecules could be carried out using a minimal basis set (STO-3G)[44] with relative energies determined from DFT calculations using larger basis sets for the molecules at STO-3G geometries. The basis sets employed were the valence double-ζ, 4-31G,[45] which has two sets of Gaussian functions for the carbon 2s and 2p and hydrogen 1s, and the valence double-ζ with polarization functions, 6-31G(d),[45,46] which adds a set of d functions on the carbon atoms. The largest nanotube model used is $C_{78}H_{20}$, which has 410 basis functions for the STO-3G geometry optimization and 742 for the 4-31G single-point energy calculation. The calculations were carried out using the Gaussian98[47] computer program on IBM R6000 and SGI R10000 workstations and a 16-node Pentium III-based Linux cluster.

Because there are no experimental thermochemical data available for functionalized fullerenes and nanotubes, even approximate determinations of heats of reaction and bond energies are useful for identifying viable functionalization reactions and likely products. The object of this work is to guide the experimental studies by identifying potential reaction products on the basis of bond strengths, heats of reaction and energy barriers. To accomplish this, the calculated adduct binding energies need only be accurate to 5−10 kcal/mol. It should be noted that the calculations by Bauschlicher[34−36] and Kudin et al.[38] used comparable methods.

Calculations were carried out to calibrate the computational protocol to establish the accuracy and limitations of our procedure. Table 1 contains the results of calibration calculations for F_2, HF, and small monofluoroalkanes. The agreement between the B3LYP/6-31G(d) calculations and experiment is good. For F_2 and HF, the error in R_e is less than 0.02 Å and the error in D_e is about 3 kcal/mol. For the monofluoroalkanes, the calculated bond dissociation energies (without zero point vibration energy correction) are about 2.5 kcal/mol greater than the experimental bond enthalpies (298 K). One would expect the bond enthalpy to be several kcal/mol smaller than the dissociation energy for these molecules. Thus we expect B3LYP/6-31G(d) calculations to yield adduct binding energies that are accurate to better than 5 kcal/mol. It can also be seen for monofluoroalkanes that carrying out energy calculations at the STO-3G optimized geometries increases the systematic error by no more than 2 kcal/mol. Thus, our choice of using B3LYP/STO-3G geometries and B3LYP/4-31G or 6-31G(d) energies is consistent with the goal of 5−10 kcal/mol accuracy in the calculations. Use of only the B3LYP/STO-3G energies would result in considerably larger errors.

TABLE 1: Comparison of B3LYP and Experimental Bond Energy Data for Fluorine-Containing Molecules[a]

molecule		STO-3G	4-31G	6-31G(d)	exp
F_2	R_e	1.37	1.47	1.40	1.41[b]
	D_e	79.0	33.5	42.2	38.2[b]
	D_e at STO-3G geometry		29.4	41.8	
HF	R_e	1.00	0.95	0.93	0.917[b]
	D_e	119.1	118.4	128.2	129.5[b]
	D_e at STO-3G geometry		117.4	126.1	
CH_3F	$D_e(CH_3-F)$	116.2	102.0	112.8	109.9[c]
	D_e at STO-3G geometry		101.3	112.0	
iso-C_3H_7F	$D_e(C-F)$	112.2	104.0	113.7	117.2[c]
C_3H_8	$D_e(>C-H)$	132.0	104.4	104.2	99.1[d]

[a] Bond lengths in Å and energies in kcal/mol. [b] Reference 48. [c] Reference 49. [d] Reference 42.

TABLE 2: Fluorine Adduct Binding Energies to C_{60}[a]

substrate and product[b]	STO-3G	4-31G	6-31G(d)
	$C_{30}H_{12}$		
E1F	−44.7	−38.0 (−40.5)[c]	−47.3
E2F *6/6*	−131.6	−111.5	−130.2
	C_{60}		
E*1*F	−55.6	−41.8	
E2F *6/6*	−141.4	−114.9	
E2F *5/6*	−120.8	−98.3	
E2F *1−3*	−87.6	−71.2	
E2F *1−4A*	−131.3	−109.9	
E2F *1−4B*	−108.4	−89.4	
E4F *6/6A*	−290.0	−239.1	
E4F *6/6B*	−280.7	−232.4	
E6F *6/6A* (“T”)	−436.0	−357.9	
E6F *6/6B* (“S”)	−439.4	−363.8	
E6F *6/6C* (“O”)	−431.5	−349.0	

[a] Energies in kcal/mol from B3LYP calculations. [b] Pattern of fluorine atoms in products given in Figure 3. [c] B3LYP/4-31G optimized geometry.

3. Results for Fullerenes

C_{60}. The first part of this work is the study of fluorination products of C_{60}. Radical addition and cycloaddition reactions of small fullerenes generally involve addition to one of the C═C double bonds radiating from a pentagon (denoted 6/6 because it forms an edge between two fused hexagons) rather than one of the C−C single bonds that comprise the perimeter of a pentagon (denoted 5/6).[50] The localized nature of the π electrons in fullerenes should make these reactions rather facile. However, considerable geometrical changes are required because the underlying carbon atoms are converted from sp^2 to sp^3 hybridization.

The results of the calculations of adduct binding energy both for the small fullerene model ($C_{30}H_{12}$) shown in Figure 1 and for C_{60} are given in Table 2. For the former, only the single F-atom adduct $C_{30}H_{12}F$ and the 6/6 addition product for a pair

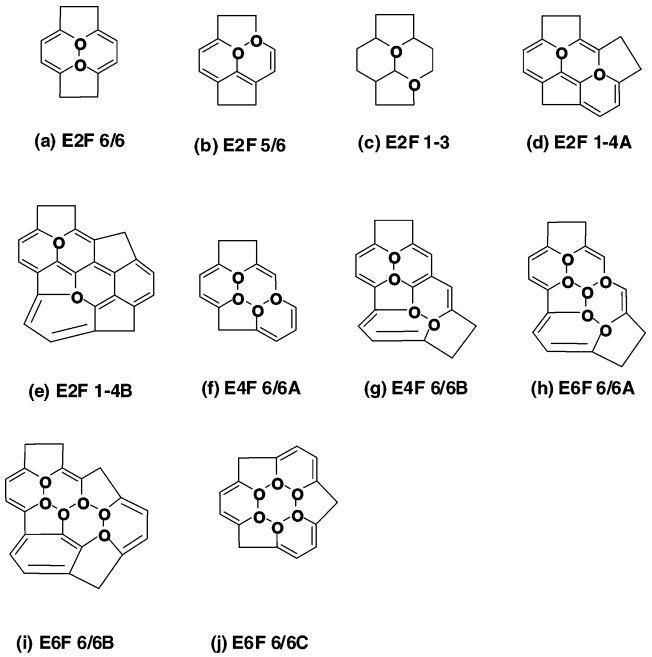

Figure 3. Patterns of fluorination for $C_{60}F_2$ (a−e), $C_{60}F_4$ (f−g), and $C_{60}F_6$ (h−j) showing rearrangement of single and double C−C bonds (except for (c) E*2*F*1*−*3*). Fluorine atoms are attached to carbon atoms marked **o**. Only part of the fullerene structure is shown. Distortions of the rings arise from the 2-dimensional projection of the curved structure.

of fluorine atoms, E*1*F and E*2*F*6/6*, respectively, are considered. For C_{60}, several $C_{60}F_2$ isomers are examined: the 6/6 and 5/6 products as well as 1−3 and 1−4 adducts in which the fluorine atoms attach to nonadjacent carbons. Figure 3 shows the pattern of fluorination considered for these calculations including the changes in double and single bonds required to form a particular addition product. Only the portion of the C_{60} substrate that exhibits changes in the normal fullerene C−C bonding pattern is shown. Other C_{60} fluorination products considered are $C_{60}F_4$ and $C_{60}F_6$ to assess the degree of additivity in the binding energies for successive fluorine pairs and to compare with the experimentally determined addition patterns.[19] It can be seen from Table 2 that the binding energies are comparable for adding two F-atoms to C_{60} and $C_{30}H_{12}$. This supports the use of small curved model molecules to represent fullerenes and nanotubes. For the single F-atom addition products, the difference in binding energies between the two models is larger, but the results are qualitatively similar in that the single F-atom binding energy is 34−39% of the double F-atom binding energy. Confirming the results of our earlier studies of fullerene and nanotube cycloaddition reactions,[33] it can be seen that for $C_{30}H_{12}F$, the use of STO-3G geometry optimization followed by energy evaluation with the 4-31G basis set leads to nearly identical adduct binding energies as would be obtained from carrying out the geometry optimization in that larger basis set (the difference between using STO-3G or 4-31G geometries for E*1*F for the small fullerene model is 2 kcal/mol). Finally, it is noted that the B3LYP/4-31G binding energy is smaller in magnitude than the B3LYP/6-31G(d) binding energy by 9 kcal/mol for E*1*F and 19 kcal/mol for E*2*F*6/6*. However, the B3LYP/STO-3G binding energies are close to the corresponding 6-31G(d) basis set binding energies.

As noted above, the binding energy for a pair of fluorine atoms in the 6/6 position is nearly 3 times the energy for a single F-atom. The 6/6 product for $C_{60}F_2$ is the most stable isomer (by 16.6 kcal/mol over the 5/6 product and 5.0 kcal/mol over the more stable of the two 1−4 products), in agreement with experiment.[18] The 6/6 product results in the loss of one π bond between pentagons whereas the other products result in loss of additional "6/6" π-bonds and formation of the same number of "5/6" π-bonds. Each 6/6 to 5/6 π-bond conversion results in a lowering of the adduct energy and, therefore, a lowering of the total fluorine binding energy. For example, the 1−4A product has one 5/6 π-bond and the 5/6 and 1−4B products have two and three 5/6 π-bonds, respectively, and increasingly smaller adduct binding energies. The bond length changes observed for the various $C_{60}F_2$ isomers are consistent with these assignments. In the calculated C_{60} geometry, 6/6 bonds between pentagons have length 1.41 Å and 5/6 bonds along the pentagon sides have length 1.48 Å. After fluorination, the three C−C bonds radiating from the substitution point lengthen to more than 1.56 Å. The neighboring bonds adjust to form short (1.38−1.41 Å) and long (1.46−1.50 Å) bonds, as indicated by double and single bonds, respectively, in Figure 3. The C−C*−C angles (C* is the attachment site) change from 108.0 and 120.0° for the pentagon and hexagon, respectively, to 100.1 and 109.8°, indicating a puckering at the substitution site as the C* carbon hybridization is converted from sp^2 to sp^3. The 1−3 product is least stable, because it is not possible to rearrange the bonding in the vicinity of the adducts to satisfy the carbon valence structure with localized C−C single and double bonds. Two of the possible $C_{60}F_4$ structures and three of the possible $C_{60}F_6$ structures are considered with different spacings between the 6/6 F-atom pairs, as shown in Figure 3. The magnitude of the fluorine binding energy per F-atom increases slightly upon addition of a second or third pair of fluorine atoms. For example, (E*2*F*6/6*)/2 = −57.4 (−70.7), (E*4*F*6/6A*)/4 = −59.8 (−72.5), and (E*6*F*6/6*)/6 = −60.6 (−73.2). All energies are in kcal/mol for B3LYP/4-31G with the STO-3G values given in parentheses. The incremental binding energy is nearly 10 kcal/mol higher in magnitude for adding the second pair, but only 0.5 kcal/mol higher for addition of the third pair. This indicates an energetic preference for clustering pairs of F-atom adducts on one side of the fullerene instead of distributing them to maximize the spacing between adducts. Evidence from experiment[19] is consistent with the assignment of E*2*F*6/6* (C_{2v} symmetry) and E*4*F*6/6A* (C_s symmetry) as the most stable structures for $C_{60}F_2$ and $C_{60}F_4$, respectively. For $C_{60}F_4$, that structure, which has the fluorine atoms added to neighboring carbon−carbon double bonds, is 7 kcal/mol more stable than E*4*F*6/6B* (also C_s symmetry), which has the fluorine pairs, separated. For $C_{60}F_6$, the so-called "T" and "S" structures are considered (C_s and C_2 symmetry, respectively) as well as a more compact structure, denoted "O", in which all the carbon atoms in one hexagon are fluorinated. These structures are labeled E*6*F*6/6A*, E*6*F*6/6B*, and E*6*F*6/6C*. The "S" structure is lowest in energy with "T" and "O" 6 and 15 kcal/mol higher, respectively. On the basis of 2-D NMR data, Boltalina et al.[19] assign the structure of $C_{60}F_6$ to the "S" isomer but surmise that the "T" form is the precursor to $C_{60}F_8$. The "T" motif is seen as well in higher fullerene fluorides such as C60F18.[12,13] It could be that both "S" and "T" isomers are formed, but the "T" more rapidly undergoes further fluorination, making it harder to isolate as a $C_{60}F_6$ intermediate.

Selected aspects of the $C_{60}F$ and $C_{60}F_2$ 6/6 product geometries and partial charges are given in Table 3. It can be seen that larger bond length changes occur for the fullerene than for the model molecule. For $C_{60}F_2$ the C−C bond connecting the reaction centers increases to 1.66 Å, whereas in the model system it is 1.57 Å. However, the other C−C bonds radiating from the substitution points are 1.58 Å in the fullerene and 1.56

TABLE 3: Single and Double (6/6) Fluorination of Fullerenes: Geometric Parameters and Partial Charges[a]

	C_{60}	$C_{30}H_{12}F$	$C_{60}F$	$C_{30}H_{12}F_2$	$C_{60}F_2$
R(C*—F)[b]		1.43	1.42	1.42	1.41
R(C*═C)[c]	1.41		1.56	1.57[d]	1.66[d]
R(C*—C)[e]	1.48		1.59	1.56	1.58
q(C*)		+0.57	+0.69	+0.43	+0.48
q(F)		−0.40	−0.51	−0.31	−0.37

[a] Bond lengths in Å from B3LYP/STO-3G geometries and CHELPG partial charges from B3LYP/4-31G calculations. [b] C* denotes carbon atom with attached fluorine. [c] C*═C is 6/6 bond connecting two pentagons. [d] Value for C*—C* bond. [e] C*—C is 5/6 bond on edge of a pentagon.

Å in the model system. The calculated C−F bond lengths are also nearly identical: 1.42 Å in $C_{60}F_2$ and 1.41 Å in $C_{30}H_{12}F_2$. Partial atomic charges have been calculated from a Mulliken analysis of the DFT wave function and from matching the electrostatic potential (EP) using the CHELPG algorithm.[51] In the latter, the electrostatic potential of the functionalized fullerene molecule is computed, from the electron density, for a 3-dimensional grid surrounding the molecule. Partial atomic charges are then determined such that the electrostatic potential generated by those charges best matches the one calculated from the electron density. An additional constraint is imposed requiring the fitted charges to reproduce the quantum chemical dipole moment of the molecule. Generally, EP partial charges provide a good representation of long-range electrostatic interactions between molecules. In this case the EP method results in highly polar C−F bonds, as evidenced by large negative fluorine charges and large positive carbon charges; however, the perturbation of carbon charges is localized around the reaction centers with very small partial charges on more distant carbon atoms. The bond polarization is also larger for the case of the singly or doubly fluorinated product than for $C_{60}F_4$ or $C_{60}F_6$. For the case of addition of a single fluorine atom, it is instructive also to examine the atomic spin densities, as the atomic centers with large spin density would be the likely sites for a second F-atom to attach. The largest spin density (0.52) is found on the carbon atom making a 6/6 pair with the reaction center, consistent with the 6/6 adduct for $C_{60}F_2$ being the most stable. The next largest spin density (0.28) is found on the two carbon atoms that represent the cis sites for the 1−4 adduct (the second most stable $C_{60}F_2$ isomer). This is consistent both with the Huckel molecular orbital (HMO) analysis of Fowler[52] that has been used to identify the substitution pattern of fullerenes on the basis of HMO bond orders and spin densities and with the EPR study of Morton et al.[53] Finally, the carbon atoms at the 1−3 product sites have a negative bond order (−0.19), perhaps indicating those sites are especially disfavored for reaction. All other carbon atoms had spin densities with absolute magnitude less than 0.12.

Large Fullerenes and Nanotube Endcaps. The endcap of a single-walled carbon nanotube is equivalent to half of a fullerene molecule. However, the diameter of C_{60} is only 6.8 Å, so it would form an endcap only for very small diameter nanotubes such as (5,5) or (9,0). For larger diameter nanotubes, the endcaps are equivalent to giant fullerenes, e.g., half of a C_{240} molecule would approximate an endcap for a (10,10) nanotube with diameter of 12.4 Å. Haddon et al.[54] suggested that C_{240} is chemically inert, because its 12 pentagons are completely isolated, leading to little alternation in bond lengths or to greater delocalization of the π-electron density. To examine the possibility of giant fullerene or nanotube endcap functionalization, we used the model molecule $C_{34}H_{14}$, shown in Figure 4, composed of a single pentagon and 10 hexagons. It is derived

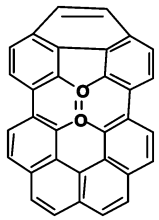

Figure 4. Model molecule ($C_{34}H_{14}$) for giant fullerenes and carbon nanotube endcaps. The attachment sites for the E*2F6/6* adduct are marked **o**.

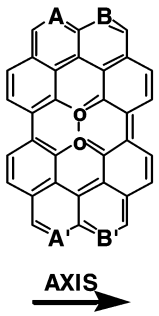

Figure 5. Small model molecule ($C_{38}H_{16}$) for (10,10) carbon nanotube. The carbon atoms marked A, B, A′, and B′ have their positions constrained to maintain the nanotube curvature (A−A′ = B−B′ = 10.006 Å). The arrow denotes the direction of the nanotube axis. Fluorine atoms in the E*2F1−2*⊥ adduct are attached to carbon atoms marked **o**.

from the smaller C_{60} model molecule by replacing one of the pentagons with a hexagon and surrounding the pentagon−hexagon core with additional hexagons.

The binding energies for one F-atom (attached at one of the pentagon vertices) and a pair of F-atoms (added to one of the C−C bonds radiating out from the pentagon) are −40.2 and −94.8 kcal/mol, respectively. For single F-atom addition, this adduct binding energy is actually 2.2 kcal/mol larger in magnitude than was found for the C_{60} model molecule. However, for the fluorine pair the adduct energy is 16.7 kcal/mol less than was found for C_{60}. The bond length changes, partial charges, and atomic spin densities are comparable to those found for C_{60}. On the basis of product stability, it appears that fluorination of giant fullerenes would be somewhat less favorable than fluorination of C_{60} itself.

4. Results for Nanotubes

To study the possible fluorination products of single-walled carbon nanotubes, curved polycyclic aromatic hydrocarbon molecules are used as model systems. These PAHs are arrays of fused hexagons, like pieces of a graphene sheet, with hydrogen atoms added around the perimeter to satisfy dangling bonds. The curvature of a cylindrical nanotube is maintained by constraining the distance between carbon atoms across the sheet so it equals the length of the chord if that molecule were part of the wall of a nanotube as shown in Figure 2. Model systems have been generated for both armchair and zigzag nanotubes. For armchair tubes, two different models for (10,-10) tubes with a diameter of 12.4 Å and one model for (5,5) tubes with a diameter of 6.6 Å are used. The smaller (10,10) model, $C_{38}H_{16}$, consists of 12 hexagons arranged in rows of 2, 3, 2, 3, 2 with curvature imposed by constraining the end carbon atoms to be 10.006 Å apart, as shown in Figure 5. For this model, the nanotube axis is parallel to the 2 and 3 hexagon rows. The larger model, $C_{64}H_{20}$, shown in Figure 2, consists of 23 hexagons in rows of 2−3−4−5−4−3−2 with the end carbon

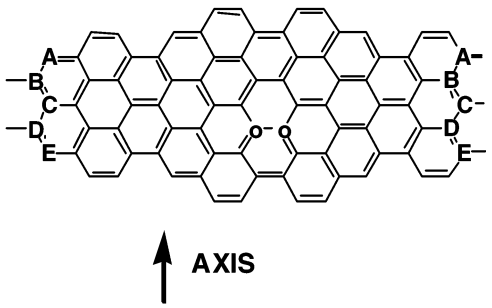

Figure 6. Model molecule ($C_{78}H_{20}$) for (5,5) carbon nanotube. The atoms labeled A−E are repeated at both sides of the molecule because the model represents a complete cross section of the nanotube. The arrow denotes the direction of the nanotube axis. Fluorine atoms in the E*2F1−2*⊥ adduct are attached to carbon atoms marked **o**.

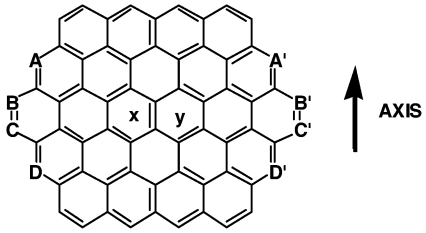

Figure 7. Model molecule ($C_{66}H_{20}$) for (16,0) carbon nanotube. The carbon atoms marked A−D have their positions constrained to maintain the nanotube curvature (A−A′ = D−D′ = 10.389 Å and B−B′ = C−C′ = 11.542 Å. The arrow denotes the direction of the nanotube axis. The central rings are marked x and y to provide reference points for the fluorine adduct locations in Figure 9.

atoms constrained to be 12.348 Å apart. This larger (10,10) model has been selected to minimize edge effects for all the fluorine adduct arrangements considered. The smaller model, though more economical for the calculations, is only suitable for addition of one or two F-atoms. The (5,5) nanotube model $C_{78}H_{20}$, shown in Figure 6, consists of 29 hexagons in arranged in rows of 2−3−2−3−4−3−4−3−2−3 and includes two complete circumferential bands of hexagons, so no constraints are needed to maintain the curvature. The zigzag nanotube model, $C_{66}H_{20}$, represents a portion of a (16,0) nanotube with diameter 12.5 Å and is shown in Figure 7. It has 24 hexagons arranged in rows of 4−5−6−5−4. It is interesting to consider both armchair and zigzag models because they have C−C bonds oriented perpendicular and parallel to the tube axis, respectively. Comparison of product energies for (10,10) and (5,5) nanotubes will also be useful in developing an understanding of curvature effects on nanotube reactivity. Both the armchair and zigzag nanotubes also have C−C bonds with skewed orientation with respect to the tube axis. Examination of fluorine addition to those bonds would also be representative of product formation for the general case of chiral nanotubes.

(10,10) and (5,5) Nanotubes. The calculated binding energies of fluorine to the armchair nanotube models are given in Table 4. For the smaller (10,10) nanotube model, only single-atom and 1−2 pair fluorine addition products are studied. For the larger model molecule, however, 1−3 and 1−4 difluoronated products and various 3- and 4-fluorine products are examined. The fluorination patterns considered are shown in Figure 8. It can be readily seen, from Table 4, that the two (10,10) nanotube models yield similar results for E*1*F and E*2F1−2*⊥, which has the fluorine atoms added across a C−C bond that lies perpendicular to the nanotube axis. The binding energy for a pair of F-atoms is almost 3 times the value for a single fluorine atom. The fluorine−nanotube binding energies are consistently smaller

TABLE 4: Fluorine Adduct Binding Energies to Armchair Nanotube Model Molecules[a]

substrate and product[b]	STO-3G	4-31G	6-31G(d)
Small (10,10) Model, $C_{38}H_{16}$			
E*1*F	−30.2	−26.9	−34.9
E*2F1−2*⊥	−95.7	−79.0	−98.1
Large (10,10) Model, $C_{64}H_{20}$			
E*1*F	−32.1	−29.0	
E*2F1−2*⊥	−92.2	−76.3	
E*2F1−2skew*	−85.3	−71.1	
E*2F1−3*	−44.9	−46.7	
E*2F1−4A*	−73.4	−64.2	
E*2F1−4B*	−72.7	−66.1	
E*3F1−2−3*	−138.4	−111.9	
E*3Ftrans*	−121.3	−100.4	
E*3Fcis*	−113.2	−96.1	
E*3Ftrig*	−96.7	−78.9	
E*4Ftrans*	−196.2	−158.4	
E*4Fcis*	−186.0	−147.4	
E*4F2+2*	−182.0	−147.2	
E*4Ftrig*	−170.9	−138.6	
(5,5) Model, $C_{78}H_{20}$			
E*1*F	−40.1	−37.7	
E*2F1−2*⊥	−107.1	−91.3	

[a] Energies in kcal/mol from B3LYP calculations. [b] Pattern of the fluorine atoms in products is given in Figure 8.

in magnitude than the values computed for C_{60}, with the difference being approximately 10−12 kcal/mol for the single atom addition and 35 kcal/mol for the fluorine pair addition. The differences between B3LYP energies with STO-3G, 4-31G, and 6-31G(d) basis sets at the STO-3G geometry are smaller than were found for fullerenes, but the same trend is observed with the magnitude of the B3LYP/4-31G binding energy being the smallest. The perpendicular orientation for the 1−2 product is favored by 5 kcal/mol over the skewed arrangement. The adduct energies for addition of two F-atoms show a preference of 10 kcal/mol for 1−2 addition over 1−4. However, the structure of the more favorable 1−4 addition product is different than the one found for $C_{60}F_2$. The 1−3 addition product is considerably less stable than any of the 1−2 and 1−4 products. Similar results are seen for the 3-F products except for E*3F1−2−3*, indicating products with noncontiguous arrangements of F-atoms are not favored. It is also seen that the binding energy for E*4Ftrans*, the most favorable 4-F addition product, is 6 kcal/mol larger in magnitude than twice E*2F1−2*⊥. Similarly, the binding energy for E*4Fcis* is larger than twice E*2F1−2skew* by 5 kcal/mol. These are indicative of an increase in binding energy for multiple pairs of fluorine atoms. Finally, the binding energy for E*4Ftrans* is 10 kcal/mol larger than E*4F2+2* and is further evidence that contiguous arrangements of fluorine atoms are favored.

Selected geometric parameters and partial charges of fluorinated armchair SWNT models are given in Table 5. The local deformations near the attachment sites are similar to those observed for fullerenes. This includes the substantial lengthening of the 1−2 C*−C bonds to 1.54−1.56 Å and the C*−C* bond to 1.64 Å. However, no π-bond localization is seen except for the "2−3" C−C bond in the 1−4 products. For the perpendicular 1−2 product, the F−F separation is 2.32 Å, which is nearly 0.7 Å larger than the underlying C−C bond length. This indicates the nanotube curvature permits the orientation of the C−F bonds to be skewed away from parallel by 27°. For the skewed 1−2 product, the F−F distance is slightly larger (2.37 Å), but the remaining geometric parameters are similar to those for the perpendicular case. The partial charges for the C* and F atoms indicate a greater charge withdrawal from the attach-

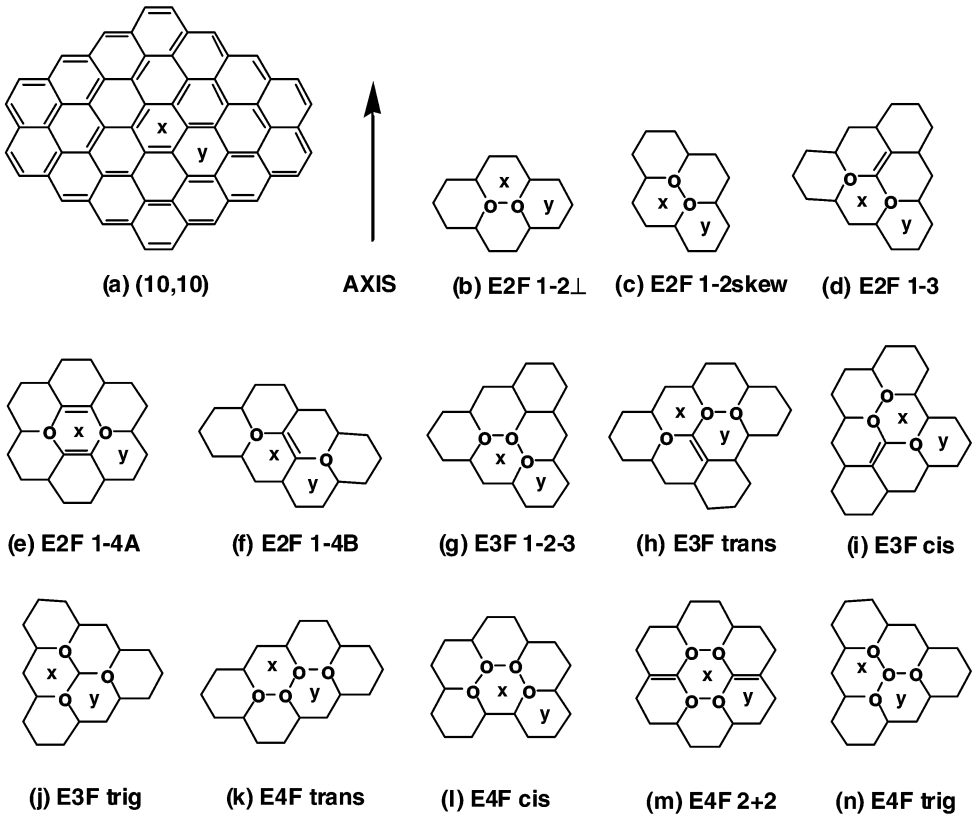

Figure 8. Patterns of fluorination for the (10,10) carbon nanotube: (a) the full model molecule with central rings marked x and y to provide reference points for the fluorine adduct locations, (b−f) doubly fluorinated adducts, (g−j) triply fluorinated adducts, and (k−n) quadruply fluorinated adducts. Fluorine atoms are attached to carbon atoms marked **o**. The only rings shown are those that have their resonant bond character disrupted. Nascent C−C double bonds are shown. The arrow denotes the direction of the nanotube axis.

ment site to neighboring carbon atoms, but less transfer to the fluorine than was seen in the case of C_{60}. For the single F-atom adduct, only half of the electron spin density is found on the adjacent carbon atoms, with most of that on the carbon that lies perpendicular to the nanotube axis. The remaining spin density is spread over the 1−4 and 1−6 carbon atoms. The sites with large spin density correlate with greater binding energies for the doubly fluorinated products.

The fluorine adduct binding energies are larger in magnitude for the (5,5) nanotube than the (10,10) by 11 kcal/mol for E*1*F and 12 kcal/mol for E*2*F*1*−*2*⊥. The structures of the fluorination products are similar for the two nanotubes. However, the 1−2 C−C bond is slightly longer in the smaller diameter case. This indicates that increased curvature leads to more stable adduct binding energies.

(16,0) Nanotubes. The calculated binding energies of fluorine to the (16,0) zigzag nanotube model are given in Table 6. The fluorination patterns considered are shown in Figure 9. For this model molecule six different 1−2 and 1−4 fluorine pair addition products have been studied, permitting a more detailed analysis of the orientation of the C−F bond pairs relative to the curvature of the nanotube. Selected geometric parameters and partial charges for these adducts are given in Table 7. For single F-atom addition, the binding energy is 2.2 kcal/mol less in magnitude than the value for the (10,10) nanotube model. However, for double F-atom addition, the binding energy of the most stable adduct (E*2*F*1*−*2*||) is 6.8 kcal/mol larger in magnitude than its (10,10) nanotube counterpart E*2*F*1*−*2*⊥. For the 1−4 adducts the binding energy difference between (16,0) and (10,10) nanotubes is even larger (16.2 kcal/mol). Furthermore, the 1−4 adduct is only 0.8 kcal/mol less stable than the 1−2. In the most stable adducts (E*2*F*1*−*2*|| and E*2*F*1*−*4*||) the fluorine

TABLE 5: Geometric Parameters and Partial Charges for Armchair Nanotube Fluorination[a]

	(10,10) model		
	small	large	(5,5) model
	Bare Substrate		
R(C*−C) ⊥[b,c]	1.42	1.41	1.44
R(C*−C) skew[c]	1.45	1.43	1.46
	Single F Adduct		
R(C*−F)	1.45	1.44	1.43
R(C*−C) ⊥	1.54	1.55	1.56
R(C*−C) skew	1.55	1.55	1.56
q(C*)	+0.91	+0.97	
q(F)	−0.41	−0.43	
	Double F Adduct, (1−2) ⊥		
R(C*−F)	1.44	1.44	1.43
R(C*−C) ⊥	1.63	1.64	1.67
R(C*−C) skew	1.55	1.55	1.54
R(F−F)	2.32	2.32	2.31
q(C*)	+0.58	+0.58	
q(F)	−0.32	−0.32	

[a] Bond lengths in Å from B3LYP/STO-3G geometries and CHELPG partial charges from B3LYP/4-31G calculations. [b] C* denotes carbon atom with attached fluorine. [c] ⊥ and skew denote C*-C bonds lying perpendicular to the tube axis (i.e., along the circumference of the tube) and skewed, respectively.

atoms are attached to neighboring carbon atoms with the C*−C* direction oriented parallel to the nanotube axis. Binding energies for adducts with the C*−C* direction skewed are about 6 kcal/mol smaller. This is similar to the findings for (10,10) nanotubes. The local deformations and partial charges near the fluorine attachment sites are similar to those seen for the (10,10) nanotube models. The magnitude of the F−F separations in the 1−2 adducts indicates that the C*−F bonds are tilted

TABLE 6: Fluorine Adduct Binding Energies to (16,0) Zigzag Nanotubes[a]

product[b]	STO-3G	4-31G
E*1*F	−28.8	−26.8
E*2*F *1−2*||	−98.5	−83.1
E*2*F *1−2 skew*	−89.6	−76.8
E*2*F *1−4*||	−94.9	−82.3
E*2*F *1−4skew1*	−87.4	−78.2
E*2*F *1−4skew2*	−60.7	−56.6
E*2*F *1−4*⊥	−68.3	−62.9

[a] Energies in kcal/mol from B3LYP calculations. [b] Pattern of fluorine atoms in products given in Figure 9.

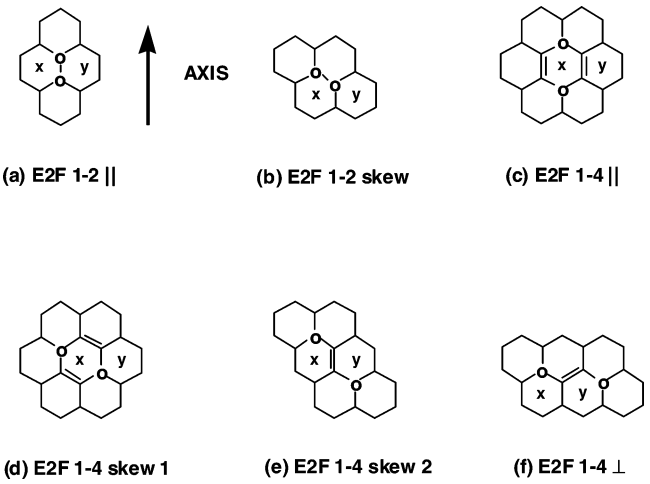

Figure 9. Patterns of double fluorination for the (16,0) carbon nanotube. Fluorine atoms are attached to carbon atoms marked **o**. The rings labeled x and y correspond to the labeled rings in Figure 7. The only rings shown are those that have their resonant bond character disrupted. Nascent C−C double bonds are shown. The arrow denotes the direction of the nanotube axis.

TABLE 7: Geometric Parameters and Partial Charges for Zigzag Nanotube Fluorination[a]

	single F adduct	double F adduct 1−2 ||	double F adduct 1−2 skew	double F adduct 1−4 ||	double F adduct 1−4 skew1
R(C*−F)[b]	1.45	1.43	1.44	1.44	1.44
R(C*−C) ||[c]	1.55	1.63[d]	1.55	1.55	1.56
R(C*−C) skew	1.55	1.56	1.64,[d] 1.55	1.56	1.56
R(F−F)		2.36	2.35		3.79
q(C*)	+0.91	+0.59		+0.81	
q(F)	−0.41	−0.33		−0.36	

[a] Bond lengths in Å from B3LYP/STO-3G geometries and CHELPG partial charges from B3LYP/4-31G calculations. [b] C* denotes carbon atom with attached fluorine. [c] || and skew denote C*-C bonds lying parallel to the tube axis and skewed, respectively. [d] Value for C*-C* bond.

away from each other. Comparison of armchair and zigzag nanotube results indicates the tube curvature facilitates the distortion of the C* bonding from trigonal to tetrahedral.

Energy Barriers. The energy barrier for migration of a fluorine adduct between adjacent carbon atoms has been computed for the larger (10,10) model system with a single F-atom adduct. The energy profiles for removal of a single fluorine atom along the surface normal were also determined for both (10,10) and (16,0) nanotubes. For the (10,10) model E*2*F*1−2* case, the barrier region of the potential energy surface for symmetric elimination of the two fluorine atoms (forming a F_2 molecule) was examined. The data for these calculations are presented in Table 8. For these calculations, the C−F bond lengths were fixed at various values and the remaining geometric degrees of freedom were optimized. In the case of F-atom migration, the fluorine atom was constrained to be at the midpoint of the migration path. For the F_2 elimination reaction, the F−F separation and orientation of the C*−F−F−C* plane were fixed and the two C*−F separations were constrained to be equal. Due to these constraints, the energy barriers, calculated at the B3LYP/4-31G level, are likely to be overestimates of the actual values. Nevertheless, they serve as qualitative indicators of the energy requirements of nanotube fluorination chemistry.

From Table 8 it can be seen that the barrier for transfer of a fluorine atom between adjacent carbon atoms is fairly high (54% of the C−F bond energy for a (10,10) nanotube). This indicates F-atom migration is unlikely to occur in fluorinated SWNTs and is in agreement with the calculations of Bauschlicher[34] for the smaller diameter (10,0) zigzag SWNT. It is uncertain if the 3.2 kcal/mol difference in barrier energies is due to nanotube curvature, chirality effects, or differences in the computational models employed. The removal of a single F-atom from the armchair nanotube model seemingly occurs without an energy barrier, whereas from the zigzag nanotube model there is a small energy barrier (14.6 kcal/mol). In the former case, when the C−F bond is extended by only 0.5 Å the spin density on the fluorine atom increases to near unity and the underlying nanotube substrate has relaxed back to its original geometry. This is indicative of the C−F bond being broken. In the latter case, however, a barrier was found for a much greater extension of the C−F bond (0.9 Å). The energy barrier for the F_2 elimination reaction pathway in the doubly fluorinated 1−2⊥ (10,10) nanotube case is quite high (only 3.0 kcal/mol less than the binding energy of the fluorine atoms). For the direct molecular fluorination reaction, this energy barrier is 30.7 kcal/mol, which is close to the dissociation of F_2, making it more likely that molecular fluorine is thermally dissociated first and that atomic fluorine reacts with the nanotubes.

5. Results for Graphene

It has been well established that fluorine gas reacts with graphite at elevated temperatures to form an intercalation product with fluorine atoms bonded to carbon atoms in all the graphene layers.[23,24] The reaction is not stoichiometric, but at temperatures between 300 and 600 °C the product composition is approximately $(C_2F)_n$ whereas at higher temperatures it is $(CF)_n$. In fact, it was this known reactivity that led to the first studies of nanotube fluorination.[20,21] To compare the reactivity of graphene and carbon nanotubes, we also carried out calculations of the single and double fluorination of a planar PAH. For this study, we used the smaller (10,10) nanotube model, which, upon geometry optimization without the curvature constraints, relaxed to a planar structure.

The binding energies for a single F-atom on the graphene model molecule calculated using the STO-3G, 4-31G, and 6-31G(d) basis sets are −22.2, −23.4, and −29.4 kcal/mol, respectively. For the 1−2 double addition product the calculated binding energies are −83.0, −71.0, and −86.6 kcal/mol, respectively for the same basis sets. The values are smaller in magnitude than the corresponding binding energies for the small (10,10) nanotube model by 3.5−8.0 kcal/mol for the single addition and 8.0−12.7 kcal/mol for the double addition. These energy differences are smallest for the 4-31G basis set and largest for the STO-3G basis set and provide an estimate of the effect of nanotube curvature on F-atom binding energy. The planar PAH molecule becomes puckered at the fluorine attach-

TABLE 8: Energy Barriers for Fluorine Atom Migration and Elimination[a]

CNT[b]	basis set	R(C−F)	R(C*−C)[c]	height[d]	ΔE_{Barr}[e]	
			1−2 Transfer			
(10,10)	4-31G	*2.1*[f]	1.47	1.97	15.6	ΔE rel to adduct
	STO-3G	*1.7*	1.51	1.52	27.1	
(10,0)	4-31G				12.4[g]	
			F Removal			
(10,10)	4-31G	*1.94*			no barrier	ΔE rel to CNT + F
(16,0)	4-31G	*2.35*	1.47		14.6	
CNT[b]	basis set	R(C−F)	R(C*−C*)	R(F−F)	ΔE_{Barr}[e]	
			F_2 Elimination			
(10,10)	4-31G	*1.9*	1.53	*1.8*	30.7	ΔE rel to CNT + F_2
	STO-3G	*1.8*	1.49	*1.4*	56.3	

[a] Bond lengths in Å from B3LYP/STO-3G geometries with constraints as noted in text. [b] Type of nanotube model. [c] C* denotes carbon atom with attached fluorine. [d] Distance from F-atom to underlying C−C bond. [e] Energies in kcal/mol. [f] Italic bond length indicates constrained value in geometry optimization. [g] ONIOM calculation from ref 34.

TABLE 9: Comparison of Binding Energies for the Most Stable Fluorination Products[a]

product	C_{60}	(10,10)	(5,5)	(16,0)	graphene
1F	−41.8	−29.0 (69)	−37.7 (90)	−26.8 (64)	−29.4 (70)
2F 1−2	−114.9	−76.3 (66)	−91.3 (79)	−83.1 (72)	−71.0 (62)
2F 1−3	−71.2	−46.7 (66)			
2F 1−4	−109.9	−66.1 (60)		−82.3 (75)	
4F	−239.1	−158.4 (66)			

[a] Energies in kcal/mol from B3LYP/4-31G calculations at B3LYP/STO-3G geometries. Values in parentheses are percentage of C_{60} binding energies.

ment sites. The local geometry changes upon F-atom addition are similar to those given in Table 5 for the small (10,10) nanotube model. However, the C*−C* and F−F distances are slightly smaller (1.62 and 2.31 Å, respectively). As noted above for the nanotube case, some of the substrate deformation that accompanies the change in C* hybridization from sp^2 to sp^3 is achieved through the nanotube curvature, making the associated energy penalty smaller for cylindrical than planar substrates and thereby increasing the binding energy.

6. Discussion

From the results presented above one can compare the fluorination products for carbon nanotubes of different diameter and chirality with those for graphite and fullerenes. The geometric changes in the substrate are similar for all cases. Bonding at the attachment carbon becomes tetrahedral and elongated due to the switch from sp^2 to sp^3 hybridization. The C−F bond length is 1.43−1.45 Å, in good agreement with experimentally determined values for fluorinated fullerenes[24] and graphite[23,24] and the C−C bonds from the attachment site to neighboring carbon atoms are elongated to 1.54−1.56 Å, typical values for C−C single bonds. However, in the 1−2 products the bonds between adjacent attachment sites are considerably elongated (1.63−1.67 Å) to help reduce steric crowding between the fluorine atoms (in these products, the F−F separation is typically 2.35 Å).

The binding energies for fluorination of C_{60} are considerably larger in magnitude than those found for graphite or nanotubes, as seen in Table 9. For double fluorination of C_{60}, the 6/6 adduct is the most stable, as expected. There is only a slight increase in the strength of the binding per F-atom adduct in the 4- and 6-fluorine atom products. Comparison of adduct binding energies for nanotubes of differing diameter and for planar graphene shows that increasing curvature increases the magnitude of the adduct binding energy. Using the results for single F-atom adducts, the binding energy is proportional to $1/R^2$, where R is the nanotube radius and for double fluorination, it is proportional to $1/R$. These relationships encompass the data for graphene ($1/R = 0$) and for (10,10), (16,0), and (5,5) nanotubes. For the B3LYP/4-31G calculations, the proportionality constants are −155.7 kcal/(mol Å^2) for single fluorination and −67.0 kcal/(mol Å) for double fluorination. For the (10,10) and (16,0) nanotubes, which have with approximately the same diameters, the binding energies of single, double, and quadruple fluorination products are 60−72% of the comparable C_{60} values. The smaller diameter (5,5) nanotube has a considerably larger single-fluorination binding energy (90% of the C_{60} value) than the other nanotube models. Thus, it appears that initiating the functionalization reaction is easier for smaller diameter nanotubes. However, the double fluorination product has only 79% of the C_{60} binding energy, indicating that this enhanced reactivity may not carry over to multiple fluorination products.

There is an interesting difference between fluorination product energies for (10,10) and (16,0) nanotubes. The latter exhibits slightly larger C−F bond strengths for the 1−2 products and significantly higher ones for the 1−4 products. In fact, for the (16,0) model molecule, the binding energies of the most stable 1-2 and 1−4 products differ by only 0.8 kcal/mol. It is generally found that 1−3 fluorination products are much less stable than 1−2 or 1−4 products. For triple and quadruple fluorination, the products are more stable if the F-atoms are attached to a series of adjacent carbon atoms (e.g., 1−2−3 or 1−2−3−4). When a single F-atom is attached to a fullerene or nanotube, an unpaired electron is generated at a neighboring carbon. It is most favorable energetically for the second F-atom to add at this site. However, the radical site can migrate to a second nearest-neighbor site, leading to a 1−4 product and the formation of a double bond between the two intervening carbon atoms. Radical migration to a nearest-neighbor site, leading to 1−3 product formation, however, results in considerable C−C bond localization into single and double bonds that is energetically unfavorable.

Most fluorination studies of graphite, fullerenes, and carbon nanotubes use the direct thermal reaction of F_2 to generate the addition products. This is a rather facile reaction owing to the low dissociation energy of molecular fluorine (38.2 kcal/mol[48]). For fullerenes, this reaction proceeds at room temperature, but for graphite and nanotubes, temperatures in excess of 300 °C are required. Table 10 gives a comparison of the energy of reaction for addition of molecular fluorine to armchair and zigzag nanotubes, C_{60}, and graphite. For comparison purposes, the energy of reaction has been divided by the number of F_2

TABLE 10: ΔE/n for the Process "Model Substrate" + nF_2 → "Model Substrate"−F_{2n}[a]

substrate	product	*n*	STO-3G	4-31G[b]	6-31G(d)
graphene model		1	−4.0	−37.5	−44.4
small fullerene model	6/6	1	−52.5	−78.0	−88.1
C_{60}	6/6	1	−62.4	−81.4	
	5/6	1	−41.7	−64.8	
	1−3	1	−8.6	−37.7	
	1−4 A	1	−52.3	−76.4	
	1−4 B	1	−29.3	−55.9	
	4F A	2	−65.9	−86.1	
	4F B	2	−61.3	−82.7	
	6F A	3	−66.3	−85.8	
	6F B	3	−67.4	−87.7	
	6F C	3	−64.8	−82.8	
giant fullerene/endcap	1−2	1	−33.0	−61.3	−71.4
(10,10) small model	1−2 ⊥	1	−16.6	−47.5	−55.9
(10,10) large model	1−2 ⊥	1	−13.1	−42.8	
	1−2 skew	1	−6.2	−37.6	
	1−3	1	+34.2	−13.2	
	1−4 A	1	+5.7	−30.7	
	1−4 B	1	+6.4	−32.6	
	3F 1−2−3	1.5	−13.2	−41.1	
	4F trans	2	−19.1	−45.7	
	4F cis	2	−13.9	−40.2	
	4F 2+2	2	−12.0	−40.1	
(5,5) model	1−2 ⊥	1	−28.0	−57.8	
(16,0) model	1−2 ||	1	−19.4	−49.6	
	1−2 skew	1	−10.5	−43.3	
	1−4 ||	1	−15.8	−48.8	
	1−4 skew1	1	−8.3	−44.7	
(10,0) ONIOM[c]	1−2 ⊥	1		−44.2	
	1−2 ||	1		−36.6	
	1−4 A	1		−30.1	
	1−4 B	1		−27.2	
	3F 1−2−3	1.5		−42.9	
	4F cis	2		−43.3	

[a] Energies in kcal/mol from B3LYP calculations. B3LYP/STO-3G geometries for fluorinated fullerenes and nanotubes except for (10,0) ONIOM calculations. [b] F_2 bond dissociation energy computed at B3LYP/4-31G geometry. [c] Reference 34.

molecules involved. It can be seen that even though the magnitudes of the adduct binding energies are considerably less for the nanotube cases than for C_{60}, all of these reactions are quite exothermic. Also, the energy of reaction per F_2 molecule is fairly insensitive to the number of fluorine molecules involved; there is a 5 kcal/mol increase in the magnitude of the binding energy per F_2 molecule between $C_{60}F_2$ and $C_{60}F_{2n}$ ($n = 2$ or 3) and a 3 kcal/mol increase for the (10,10) nanotube model. Qualitatively, Bauschlicher's ONIOM calculations for a (10,0) zigzag nanotube[34] are in agreement with the present study. The 1−2 double fluorination product is favored over the 1−4 and there is little change in binding energy per F_2 molecule for double and quadruple addition. However, the binding energies in the ONIOM calculations are somewhat smaller than the results for the larger diameter (16,0) zigzag tube in the present study, and one would expect the fluorine binding energy to increase with decreasing nanotube diameter. The semiempirical molecular orbital calculations for fluorinated fullerenes[27] and carbon nanotubes[26] report binding energies in good agreement with the B3LYP/4-31G results (e.g., the energies of reaction for $C_{60} + F_2$ are −86.0 and −81.8 kcal/mol for the 1−2 and 1−4 products, respectively, compared with values of −81.0 and −76.4 kcal/mol in the present study). However, the reported C−F bond lengths are significantly shorter (1.38 Å compared to 1.43−1.45 Å in the present study).

As the present study is limited to attachment of up to six fluorine atoms to C_{60} or carbon nanotube model molecules, it is difficult to draw comparisons with studies of highly fluorinated fullerenes and nanotubes. For armchair nanotubes, the relative energies of quadruply fluorinated products favor attachment to a series of adjacent carbon atoms with a zigzag arrangement (|E*4*Ftrans | > |E*4*Fcis|). If subsequent fluorination follows the same pattern, it will lead to strings of attached fluorine atoms either running perpendicular to the tube axis or forming helices around the nanotube. The fact that |E*2*F*1*−*2*⊥| > |E*2*F*1*−*2skew* | suggests that the initial F_2 addition will occur at a C−C bond perpendicular to the tube axis, which would start a helical pattern of F-atom addition. For zigzag nanotubes, the fact that E*2*F*1*−*2*|| and E*2*F*1*−*4*|| are comparable suggests that fluorine atoms will be added in lines parallel to the tube axis. These results differ from the conclusions of Kudin et al.[38] for periodic C_2F fluorinated nanotube models. They found the parallel zigzag arrangement most stable for armchair nanotubes and a helical one most stable for zigzag tubes. However, neither scenario is consistent with the banded patterns attributed to the fluorination products in the STM images of Halas and coworkers.[26]

7. Conclusions

In the present work, B3LYP calculations have been employed to study the reaction of small fullerenes and carbon nanotubes with molecular fluorine with a focus on the addition of one to four F-atoms to the fullerene or nanotube substrates. Most of the calculations for fullerenes are carried out for C_{60}. The nanotube substrates are represented by model polycyclic aromatic hydrocarbons that are constrained to have nonplanar geometries with curvatures corresponding to (10,10), (5,5), and (16,0) nanotubes. The preferred binding site for the second fluorine adduct is at a carbon atom adjacent to the first attachment site. The binding energy of fluorine atoms to C_{60} is about 40−50% larger than to any of the nanotube model molecules. Zigzag nanotubes are found to form more stable fluorination products than armchair ones due to a more favorable orientation of the C−C bonds relative to the nanotube axis. The reactions of F_2 with the carbon substrates are confirmed to be quite exothermic. Only a slight nonadditivity is observed for the binding energy for addition of a second pair of fluorine atoms to the fullerene or nanotube. The barriers for addition of a single fluorine atom and a F_2 molecule have been determined from the calculations. The molecular fluorine addition barrier is quite high, indicating that an atomic addition mechanism is more likely to occur under the experimental conditions employed for fullerene and nanotube fluorination.

References and Notes

(1) Kroto, H. W.; Heath, J. R.; O'Brien, S. C.; Curl, R. F.; Smalley, R. E. *Nature* **1985**, *318*, 162.
(2) Iijima, S. *Nature* **1991**, *354*, 56.
(3) Bethune, D. S.; Kiang, C. H.; de Vries, M. S.; Gorman, G.; Savoy, R.; Vasquez, J.; Beyers, R. *Nature* **1993**, *363*, 605.
(4) Okita, S.; Ishikawa, M.; Miura, K. *Surf. Sci.* **1999**, *442*, L959.
(5) Tanigaki, K.; Ebbesen, T. W.; Saito, S.; Mizuki, J.; Tsai, J.; Kubo, Y.; Kuroshima, S. *Nature* **1991**, *352*, 222.
(6) Dugan, L. L.; Turetsky, D. M.; Du, C.; Lobner, D.; Wheeler, M.; Almli, C. R.; Shen, K.-F.; Luh, T.-Y.; Choi, D. W.; Lin, T.-S. *Proc. Natl. Acad. Sci.* **1997**, *94*, 9434.
(7) Postma, H. W. C.; Teepen, T.; Yao, Z.; Grifoni, M.; Dekker, C. *Science* **2001**, *293*, 76.
(8) Qian, D.; Dickey, E. C.; Andrews, R.; Rantell, T. *Appl. Phys. Lett.* **2000**, *76*, 2868.
(9) Fowler, P. W.; Manolopoulos, D. E. *An Atlas of Fullerenes*; Clarendon Press: Oxford, U.K., 1995.
(10) Sliwa, W. *Fullerene Sci. Technol.* **1995**, *3*, 243.
(11) Krusic, P. J.; Wasserman, E.; Keizer, P. N.; Morton, J. R.; Preston, K. F. *Science* **1991**, *254*, 1183.
(12) Taylor, R. *Chem. Eur. J.* **2001**, *7*, 4075.
(13) Boltalina, O. V. *J. Fluorine Chem.* **2000**, *101*, 273.

(14) Okino, F.; Touhara, H.; Seki, K.; Mitsumoto, R.; Shigematsu, K.; Achiba, Y. *Fullerene Sci. Technol.* **1993**, *1*, 425.
(15) Boltalina, O. V.; Abdul-Sada, A. K.; Taylor, R. *J. Chem. Soc.* **1995**, 981.
(16) Boltalina, O. V.; Borschevskii, A. Ya.; Sidorov, L. N.; Street, J. M.; Taylor, R. *Chem. Commun.* **1996**, 529.
(17) Boltalina, O. V.; Sidorov, L. N.; Sukhanova, E. V.; Sorokin, I. D. *Chem. Phys. Lett*. **1994**, *230*, 567.
(18) Boltalina, O. V.; Lukonin, A. Yu.; Street, J. M.; Taylor, R. *Chem. Commun*. **2000**, 1601.
(19) Boltalina, O. V.; Darwish, A. D.; Street, J. M.; Taylor, R.; Wei, X.-W. *J. Chem. Soc., Perkin Trans. 2* **2002**, 251.
(20) Hamwi, A.; Alvergnat, H.; Bonnamy, S.; Beguin, F. *Carbon* **1997**, *35*, 723.
(21) Mickelson, E. T.; Huffman, C. B.; Rinzler, A. G.; Smalley, R. E.; Hauge, R. H.; Margrave, J. L. *Chem. Phys. Lett.* **1998**, *296*, 188.
(22) Mickelson, E. T.; Chiang, I.; Zimmerman, J. L.; Boul, P. J.; Lozano, J.; Liu, J.; Smalley, R. E.; Hauge, R. H.; Margrave, J. L. *J. Phys. Chem. B* **1999**, *103*, 4318.
(23) Kamarchik, P.; Margrave, J. L. *Acc. Chem. Res*. **1978**, *11*, 296.
(24) Hamwi, A. *J. Phys. Chem. Solids* **1996**, *57*, 677.
(25) Boul, P. J.; Liu, J.; Mickelson, E. T.; Huffman, C. B.; Ericson, L. M.; Chiang, I. W.; Smith, K. A.; Colbert, D. T.; Hauge, R. H.; Margrave J. L.; Smalley, R. E. *Chem. Phys. Lett.* **1999**, *310*, 367.
(26) Kelly, K. F.; Chiang, I. W.; Mickelson, E. T.; Hauge, R. H.; Margrave, J. L.; Wang, X.; Scuseria, G. E.; Radloff, C.; Halas, N. J. *Chem. Phys. Lett*. **1999**, *313*, 445.
(27) Matsuzawa, N.; Fukunaga, T.; Dixon, D. A. *J. Phys. Chem.* **1992**, *96*, 10747.
(28) Clare, B. W.; Kepert, D. L. *J. Mol. Struct. (THEOCHEM)* **2002**, *589*−*590*, 209.
(29) Clare, B. W.; Kepert, D. L. *J. Mol. Struct. (THEOCHEM)* **2002**, *583*, 19.
(30) Austin, S. J.; Fowler, P. W.; Sandall, J. P.; Birkett, P. R.; Avent, A. G.; Darwish, A. D.; Kroto, H. W.; Taylor, R.; Walton, D. R. M. *J. Chem. Soc., Perkin Trans. 2* **1995**, 1027.
(31) Fowler, P. W.; Sandall, J. P. B. *J. Chem. Soc., Perkin Trans. 2* **1995**, 1247.
(32) Cahill, P. A.; Rohlfing, C. M. *Tetrahedron* **1996**, *52*, 5247.
(33) Jaffe, R. L. Quantum Chemistry Study of Chemical Functionalization Reactions of Fullerenes and Carbon Nanotubes. In *Fullerenes Vol. 7: Recent Advances in the Chemistry and Physics of Fullerenes and Related Materials*; Kamat, P. V., Guldi, D. M., Kadish, K. M., Eds.; Electrochemical Society: Pennington, NJ, 1999; p 153.
(34) Bauschlicher, C. W. *Chem. Phys. Lett*. **2000**, *322*, 237.
(35) Bauschlicher, C. W. *Nano Lett.* **2001**, *1*, 223.
(36) Bauschlicher, C. W.; So, C. R. *Nano Lett.* **2002**, *2*, 337.
(37) Svensson, M.; Humbel, S.; Froese, R. D. J.; Matsubara, T.; Sieber, S.; Morokuma, K. *J. Phys. Chem.* **1996**, *100*, 19357.
(38) Kudin, K. N.; Bettinger, H. F.; Scuseria, G. E. *Phys. Rev. B* **2001**, *63*, 045413.
(39) Han, J.; Jaffe, R. *J. Chem. Phys.* **1998**, *108*, 2817.
(40) Lee, C.; Yang, W.; Parr, R. G. *Phys. Rev. B* **1988**, *37*, 785.
(41) Becke, A. D. *J. Chem. Phys*. **1993**, *98*, 5648.
(42) Stephens, P. J.; Devlin, F. J.; Chabalowski, C. F.; Frisch, M. J. *J. Phys. Chem.* **1994**, *98*, 11623.
(43) Afeefy, H. Y.; Liebman, J. F.; Stein, S. E. Neutral Thermochemical Data. In *NIST Chemistry WebBook*; NIST Standard Reference Database Number 69; Linstrom, P. J., Mallard, W. G., Eds.; National Institute of Standards and Technology: Gaithersburg MD, 20899, July 2001 (http://webbook.nist.gov).
(44) Hehre, W. J.; Stewart, R. F.; Pople, J. A. *J. Chem. Phys.* **1969**, *51*, 2657.
(45) Ditchfield, R.; Hehre, W. J.; Pople, J. A. *J. Chem. Phys.* **1971**, *54*, 724.
(46) Hariharan, P. C.; Pople, J. A. *Theor. Chim. Acta* **1973**, *28*, 213.
(47) Frisch, M. J.; Trucks, G. W.; Schlegel, H. B.; Scuseria, G. E.; Robb, M. A.; Cheeseman, J. R.; Zakrzewski, V. G.; Montgomery, J. A., Jr.; Stratmann, R. E.; Burant, J. C.; Dapprich, S.; Millam, J. M.; Daniels, A. D.; Kudin, K. N.; Strain, M. C.; Farkas, O.; Tomasi, J.; Barone, V.; Cossi, M.; Cammi, R.; Mennucci, B.; Pomelli, C.; Adamo, C.; Clifford, S.; Ochterski, J.; Petersson, G. A.; Ayala, P. Y.; Cui, Q.; Morokuma, K.; Malick, D. K.; Rabuck, A. D.; Raghavachari, K.; Foresman, J. B.; Cioslowski, J.; Ortiz, J. V.; Stefanov, B. B.; Liu, G.; Liashenko, A.; Piskorz, P.; Komaromi, I.; Gomperts, R.; Martin, R. L.; Fox, D. J.; Keith, T.; Al-Laham, M. A.; Peng, C. Y.; Nanayakkara, A.; Gonzalez, C.; Challacombe, M.; Gill, P. M. W.; Johnson, B. G.; Chen, W.; Wong, M. W.; Andres, J. L.; Head-Gordon, M.; Replogle, E. S.; Pople, J. A. *Gaussian 98*, revision A.7; Gaussian, Inc.: Pittsburgh, PA, 1998.
(48) Huber, K. P.; Herzberg, G. *Molecular Spectra and Molecular Structure IV. Constants of Diatomic Molecules*; Van Nostrand-Reinhold: New York, 1979.
(49) Luo, Y.-R.; Benson, S. W. *J. Phys. Chem. A* **1997**, *101*, 3042.
(50) Meier, M. S.; Wang, G.-W.; Haddon, R. C.; Brock, C. P.; Lloyd, M. A.; Selegue, J. P. *J. Am. Chem. Soc.* **1998**, *120*, 2337.
(51) Breneman, C. M.; Wiberg, K. B. *J. Comput. Chem.* **1990**, *11*, 361.
(52) Rogers, K. M.; Fowler, P. W. *J. Chem. Soc., Chem. Commun*. **1999**, 2357.
(53) Morton, J. R.; Preston, K. F.; Negri, F. *Chem. Phys. Lett.* **1994**, *221*, 59.
(54) Haddon, R. C.; Scuseria, G. E.; Smalley, R. E. *Chem. Phys. Lett.* **1997**, *272*, 38.